Analysis and characterization of thermal transport in GaN HEMTs on Diamond substrates

Conference Paper · May 2014

DOI: 10.1109/ITHERM.2014.6892416

Analysis and Characterization of Thermal Transport in GaN HEMTs on Diamond Substrates

David Altman[1], Matthew Tyhach[1], James McClymonds[1], Samuel Kim[2], Samuel Graham[2], Jungwan Cho[3], Kenneth Goodson[3], Daniel Francis[4], Firooz Faili[4], Felix Ejeckam[4], and Steven Bernstein[1]
[1] Raytheon Integrated Defense Systems, Sudbury, MA 01776
[2] Georgia Institute of Technology, Atlanta, GA 30332
[3] Stanford University, Stanford, CA 94305
[4] Element Six Technologies, Santa Clara, CA 95054
david_h_altman@raytheon.com

ABSTRACT

The emergence of Gallium Nitride-based High Electron Mobility Transistor (HEMT) technology has proven to be a significant enabler of next generation RF systems. However, thermal considerations currently prevent exploitation of the full electromagnetic potential of GaN in most applications, limiting HEMT areal power density (W/mm^2) to a small fraction of electrically limited performance. GaN on Diamond technology has been developed to reduce near junction thermal resistance in GaN HEMTs. However, optimal implementation of GaN on Diamond requires thorough understanding of thermal transport in GaN, CVD diamond and interfacial layers in GaN on Diamond substrates, which has not been thoroughly previously addressed.

To meet this need, our study pursued characterization of constituent thermal properties in GaN on Diamond substrates and temperature measurement of operational GaN on Diamond HEMTs, employing electro-thermal modeling of the HEMT devices to interpret and relate data. Strong agreement was obtained between simulations and HEMT operational temperature measurements made using two independent thermal metrology techniques, enabling confident assessment of peak junction temperature. The results support the potential of GaN on Diamond to enable a 3X increase in HEMT areal dissipation density without significantly increasing operational temperature. Such increases in HEMT power density will enable smaller, higher power density Monolithic Microwave Integrated Circuits (MMICs).

KEY WORDS: High Electron Mobility Transistor, CVD Diamond, Micro-Raman Thermography, Gate Thermometry, Electro-thermal Modeling

INTRODUCTION

Self-heating effects are well known to limit power density in GaN on SiC HEMT-based MMICs. While RF power densities as high as 40W/mm [1] and HEMT gate-to-gate spacings as small as 10µm have each been demonstrated, thermally-induced performance and reliability degradation in modern GaN MMICs must generally be mitigated by reducing drain voltage and/or increasing gate-to-gate spacing.

To address this thermal limitation and to provide a path to higher power density devices, techniques to integrate polycrystalline diamond in close proximity to the junction have been developed [2]. By employing CVD diamond (in lieu of SiC) to spread heat within microns of the junction, GaN on Diamond technology seeks to address limitations associated with near junction thermal resistance in GaN HEMTs without impacting substrate electrical properties [3].

GaN on Diamond composite substrates are fabricated through chemical vapor deposition (CVD) diamond growth on flipped GaN epitaxial layers coated with a proprietary dielectric [4]. As such, the properties of both the substrate and interfacial layers found in GaN on Diamond substrates are markedly different than those present in GaN on SiC or GaN on Si substrates [5].

Thermal characterization of HEMT devices fabricated using GaN on Diamond has been performed, with results indicating thermal performance benefits [6]; however, the material characteristics that govern device thermal performance have not been thoroughly studied and related to the measured benefit. Such an assessment is critical to building confidence in the thermal benefits associated with GaN on Diamond and enabling thermally-informed GaN on Diamond RF device design.

EXPERIMENTAL METHODS AND APPROACH

This study focused on: 1) systematic characterization of constituent thermal properties in GaN on Diamond substrates; 2) measurement of operational temperature in HEMT devices on GaN on Diamond substrates using two independent methods and 3) electro-thermal modeling of HEMT devices to interpret and relate data from these thermal property and operational temperature measurements. Descriptions of the GaN on Diamond substrate and HEMT fabrication processes can be found in [2-4].

Characterization of Constituent Thermal Properties in GaN on Diamond Substrates

Characterization of thermal properties of GaN on Diamond substrates was performed using a combination of Time-Domain Thermo-Reflectance (TDTR) and one-dimensional steady-state (1DSS) measurements. These measurements focused primarily on the GaN epitaxial layer and Thermal Interface Resistance (TIR) associated with the dielectric adhesion layer, heterogeneous interface resistances, and near-interface conductivity gradients in the CVD diamond film, herein referred to as "first-to-grow" CVD diamond.

TDTR Measurements of GaN Conductivity and GaN-Diamond TIR.

Picosecond TDTR measurements were performed at Stanford University to characterize GaN epitaxial layer and GaN-substrate Thermal Interface Resistance (TIR). The TIR measurement approach and data fitting method employed provided combined assessment of the thermal resistance of the dielectric film, heterogeneous interface resistances and "first to grow" CVD diamond properties.

Samples were prepared by etching the GaN buffer layer to three characteristic thicknesses ranging from ~500 to 1500nm

and applying a 50nm aluminum transducer to the top of the GaN (Figure 1).

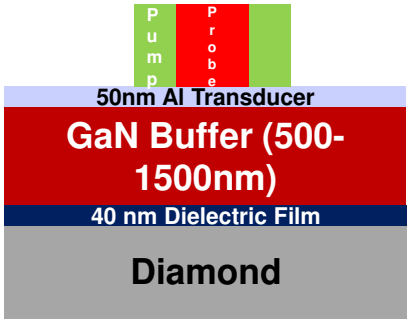

Fig.1 Sample configuration for TDTR measurement of GaN on Diamond TIR

The measurement was performed using an Nd:YVO_4 laser emitting picosecond duration pulses to both heat the Al transducer and measure reflectance following heating. Reflectance was then related to temperature based upon the linear relationship between temperature and reflectivity. A 3D radial symmetric heat diffusion solution was fitted to the normalized temperature decay data using a least-squares algorithm to extract the properties of the multi-layer stack [7].

Room temperature measurements of GaN conductivity were supplemented with temperature-dependent measurements taken from 300-550K reported in [5]. Since strong thermal conductivity gradients are anticipated in CVD diamond due to the columnar grain growth and coalescence [8], measurements focused on extraction of GaN-diamond TIR were performed with multiple pulsing frequencies, varying the thermal penetration depth within the sample. In all measurements, layer thicknesses were verified through a combination of cross-section SEM and TEM measurements.

One-Dimensional Steady State Measurements of Diamond Conductivity.

One-dimensional steady state measurements were performed based upon the method described in [9] to obtain in-plane thermal conductivity of the CVD diamond substrate. Samples were prepared through CVD growth of 50µm thick, ~10 x 45mm free-standing diamond films. A miniature film heater, air-cooled heat sink and precisely located Type-K thermocouples were employed to heat and cool the sample within an enclosure suppressing convective and radiative losses. Temperature measurements were conducted with known heating conditions and linear regression was performed to extract in-plane CVD diamond thermal conductivity.

Measurement of GaN on Diamond HEMT Operational Temperature

Gate Thermometry [10] and Micro-Raman Thermography [11] measurements were performed at Raytheon and Georgia Tech, respectively, to measure operational temperatures in GaN on Diamond HEMTs.

These measurements were performed on 10 x 125µm HEMT devices fabricated using Raytheon's microwave GaN process on early generation GaN on Diamond substrates. The devices fabricated were on a ~94µm CVD diamond substrate with 10 and 40µm gate-to-gate spacing (Figure 2).

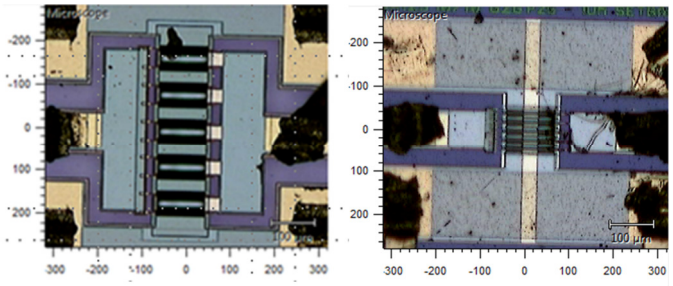

Fig.2 40µm (left) and 10µm (right) gate-to-gate spacing 10 x 125µm GaN HEMTs

Figure 3 shows the general test device layout and fixturing approach employed for thermal testing. Each singulated die featured multiple HEMTs, and they were attached to a 0.015" thick spreader tab using standard AuSn solder attach. The spreader tab was attached using a thermal epoxy to a CuMo center bar. The center bar was attached to an aluminum plate bolted to a temperature controlled stage.

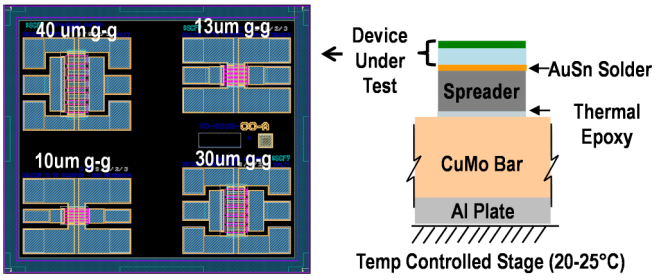

Fig.3 Layout of HEMTs on test die (left) and configuration employed in thermal measurements (right)

Gate Thermometry Measurements of HEMT Effective Temperature.

Gate Thermometry measurements were performed to obtain an "effective temperature" over the gate-channel interface of the HEMT. The measurement was performed using a high speed pulsing circuit to measure gate forward bias voltage immediately following the removal of dissipated power. The measured forward gate bias voltage was then related to temperature through a calibration curve. Steady-state device temperature was determined by fitting the measured temperature decay data to a transient analysis of the fixtured device using the device finite element thermal model.

Micro-Raman Measurements of Local HEMT Temperature.

Micro-Raman measurements were performed to obtain local temperature at various optically accessible locations in the GaN on Diamond HEMT. Micro-Raman measurements provided locally resolved channel temperature within the GaN film during DC-bias operation. All measurements were performed by first calibrating the Raman signature to a fixed stage temperature and then biasing the device to a known dissipation. The shift in Raman signature, specifically the A1(LO) peak, was characterized and data reduction was performed using calibration data and experimentally determined temperature-phonon frequency relations, similar as described in [12].

Electro-thermal Modeling of HEMT Devices

Electro-thermal modeling was performed to relate thermal property and operational temperature measurements and to assess peak junction temperature in the fabricated GaN on Diamond HEMTs.

To perform these simulations, detailed finite element models were constructed in ANSYS TAS of the fixtured HEMT devices. These models employed the aforementioned GaN on Diamond thermal properties, along with independently measured fixture thermal properties (e.g., AuSn solder, spreader tab, epoxy, CuMo). All thermal properties were held consistent in all models, and no additional fitting parameters were employed.

Device geometry was defined based upon Raytheon's microwave GaN transistor process and electro-thermal simulations were performed in Silvaco Blaze to determine detailed local heating profiles at the two-dimensional electron gas (2DEG) interface. Steady state simulations were performed for comparison to Micro-Raman data and to determine peak junction temperatures. Transient simulations were performed for comparison to Gate Thermometry temperature data and to determine extrapolated steady-state effective HEMT temperature.

RESULTS AND DISCUSSION

Constituent Thermal Properties in GaN on Diamond Substrates

GaN on Diamond substrate thermal properties were measured using the aforementioned methods and approach. As appropriate, regression analysis was performed on temperature dependent data, resulting in the values shown in Table 1.

GaN conductivity and GaN-diamond TIR data were acquired by simultaneously fitting TDTR data for each varying GaN thickness sample under the assumption that the GaN conductivity and GaN-Diamond TIR do not vary appreciably from sample to sample (Figure 4). Literature values for Al (2.4MJ/m^{3}K) [13], GaN (2.6MJ/m^{3}K) [14] and Diamond (1.8MJ/m^{3}K) [15] volumetric heat capacity were employed in data reduction. Prior work [16, 17] has shown this to be a valid approach for TDTR data reduction with fully dense materials.

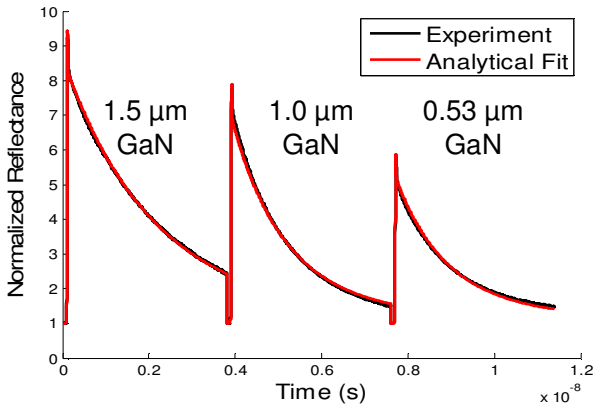

Fig.4 Fitted TDTR data for GaN on Diamond substrate samples with varying GaN thickness

GaN on Diamond TIR = $R_{GaN\text{-}Dielectric} + R_{Dielectric} + R_{Dielectric\text{-}Diamond} + R_{\text{"first to grow" Diamond}}$ was found to be 47.6m^2-K/GW at room temperature. The thermal penetration depth at 2MHz corresponds to approximately 3µm in GaN (assuming k_{GaN} = 150W/mK), thus the thermal penetration is expected to be great enough to capture the near-interfacial diamond region. This conclusion was also confirmed by fitting the data at multiple modulation frequencies. There was essentially no difference observed in the extracted TIR when fitting at 2 and 8MHz. Given that the effective thermal penetration depth (for the dielectric film) at 2MHz is twice that at 8MHz, this result further supports the assertion that the measurement was effectively capturing the effect of "first to grow" diamond thermal conductivity gradients as part of the measured TIR.

The GaN conductivity obtained in the data fit was compared to and exhibited reasonable agreement with data reported in [5]. An uncertainty in GaN-Diamond TIR of ±4m^2-K/GW was determined based upon a 10% uncertainty in Al transducer thickness. Sensitivity analysis was performed for assumed isotropic diamond conductivities ranging from 400 to 2169W/mK, resulting in variations in TIR less than the aforementioned uncertainty. While the measured GaN-Diamond TIR is notably higher than the 4-5m^2-K/GW room temperature value observed in GaN on SiC substrates in [18], it is within the range of many other GaN-substrate TIRs reported in [19].

1DSS-acquired in-plane CVD diamond conductivity was found to vary from 1281-1350W/mK in multiple samples at room temperature. A temperature dependence of $T^{-0.55}$ and anisotropy of 20% was assumed based upon results reported by Sukhadolau [20] and Coe and Sussman [21] of similar purity diamond films. Thermal properties employed for packaging layers were obtained via laser flash measurements and using resistance thermometry methods at Raytheon.

Table 1. Nominal constituent thermal properties obtained through independent measurement

Property	Value (T in Kelvin)
GaN Conductivity (W/mK)	$490560*T^{-1.41}$
GaN-Dia. TIR (m^2-K/GW)	47.6
Diamond Conductivity (W/mK, in plane)	$27287*T^{-0.55}$
Diamond Conductivity (W/mK, through plane)	$34109*T^{-0.55}$
AuSn Solder R_{th} (mm^2-K/W)	0.45
Spreader Conductivity (W/mK)	140
Epoxy R_{th} (mm^2-K/W)	5.5
CuMo Conductivity (W/mK)	167

Gate Thermometry Measurements of GaN on Diamond HEMT Operational Temperature

Gate Thermometry measurements were taken for GaN on Diamond HEMTs with 10 and 40µm gate-to-gate spacing and GaN on SiC HEMTs with 30um and 40um gate-to-gate spacing, all at P_{diss} = 6.9W/mm. Measured temperature decay data was compared to the modeled HEMT thermal response to enable extrapolation of steady-state HEMT effective temperature (Figure 5).

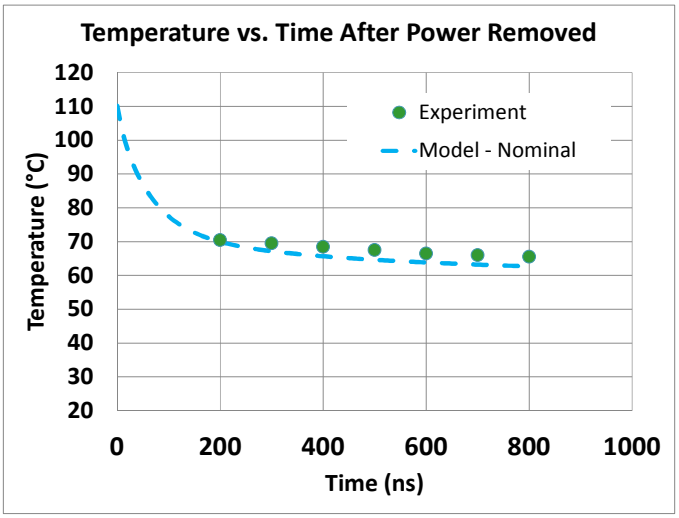

Fig.5 Experimental and modeled temperature decay data for GaN on Diamond HEMT

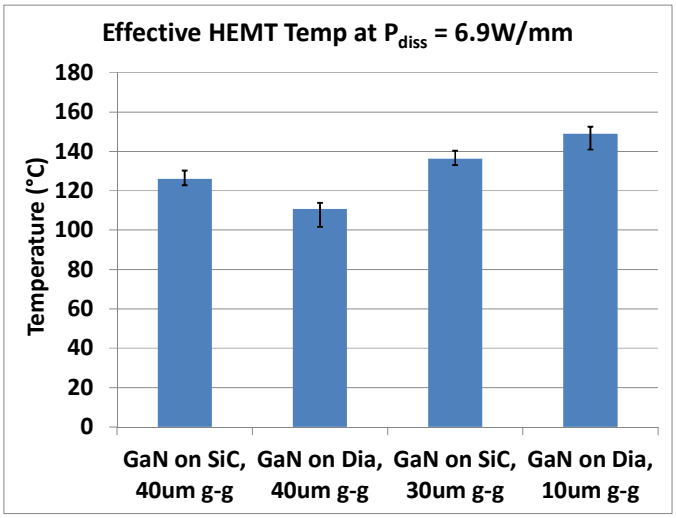

Fig.6 Comparison of effective HEMT temperatures for GaN on SiC and GaN on Diamond HEMTs

Since the gate thermometry data was collected starting 200ns following removal of dissipated power, the temperature at t = 0s was determined using the electro-thermal model. Uncertainty in the extrapolated steady-state HEMT temperature change during the first 200ns following removal of DC bias was calculated based upon uncertainty in measured properties. In these simulations, thermal conductivity variations were taken as ±10% for the Diamond substrate and GaN, and TIR uncertainty was taken as ±4m^2-K/GW for the GaN-diamond interface. These property uncertainties resulted from variation in the thickness of the Al transducer, which is usually the dominant source of uncertainty in TDTR measurements. Uncertainties in packaging layers were not considered, as they were not a determinant of the thermal behavior of the HEMT during the first 1000ns following removal of dissipated power.

Gate Thermometry measurements were performed for a 10µm gate-to-gate spacing GaN on Diamond HEMT, as well as 30 and 40µm gate-to-gate spacing 10 x 125µm GaN on SiC HEMTs measured using the same method and packaging configuration, discussed in more detail elsewhere [22].

As shown in Figure 6, these results indicate that for 40µm gate-to-gate spacing at P_{diss} = 6.9W/mm, the effective HEMT temperature of the GaN on Diamond HEMT is nominally 15.4°C cooler than the GaN on SiC HEMT. The GaN on Diamond HEMT with 10µm gate-to-gate spacing is nominally 12.7°C hotter than the GaN on SiC HEMT with 30µm gate-to-gate spacing. With a 3X higher areal heat dissipation density than the 30µm gate-to-gate spacing GaN on SiC HEMT (690 vs. 230W/mm^2), the 10µm gate-to-gate spacing GaN on Diamond HEMT was found to exhibit a 2.7X lower thermal resistance (mm^2-K/W) than the GaN on SiC device, enabling operation with the observed incremental temperature rise.

Follow-on TIR measurements on next-generation GaN on Diamond substrates indicate that a GaN-Diamond TIR of ~29m^2-K/GW can be realized. This is expected to result in a >3X reduction in thermal resistivity and equivalent or lower operating temperatures for a GaN on Diamond HEMT at 3X the areal dissipation density of GaN on SiC.

Micro-Raman Measurements of GaN on Diamond HEMT Operational Temperature

Micro-Raman measurements were taken for a 10 x 125µm GaN on Diamond HEMT with 10µm gate-to-gate spacing for dissipations varying from 1.5 to 6.9W/mm. These measurements were taken for multiple gate fingers at varying locations along the gate finger to provide a "thermal map" of the HEMT.

Measurements were taken between the gate and the drain. Modeled temperatures were determined by interrogating a 1µm^3 volume starting at the surface of the GaN buffer in the specified measurement location. The same electro-thermal models used to determine steady-state temperature in the Gate Thermometry measurements were employed to compare simulated and Micro-Raman measured local temperatures in the HEMT. The aforementioned uncertainties in material properties were used to calculate "high", "nominal" and "low" tolerance simulated temperatures to bound the model-predicted temperature range for each data point. These "high", "nominal", and "low" tolerance simulations were performed with GaN, TIR, diamond properties corresponding to the maximum and minimum values possible given the aforementioned measurement uncertainties.

Uncertainty in the Micro-Raman measured temperature value was driven by temperature phonon frequency coefficient and peak shift quantification uncertainties and did not account for measurement location variability. However, repeatability measurements were conducted to ensure the measurement locational uncertainty (along with any other repeatability-impacting uncertainties) was less than the aforementioned quantifiable uncertainties.

Figure 7 shows the measured vs. modeled comparison for various gate fingers at the edge of the gate location. These measurements were taken approximately 5µm from the edge of each gate finger. As can be observed from Figure 7 and subsequent Figures 8-10, model/experiment agreement was consistently observed to be within the bounds of simulation uncertainties, with the vast majority of measured values

matching nominal simulated results when accounting for measurement uncertainty.

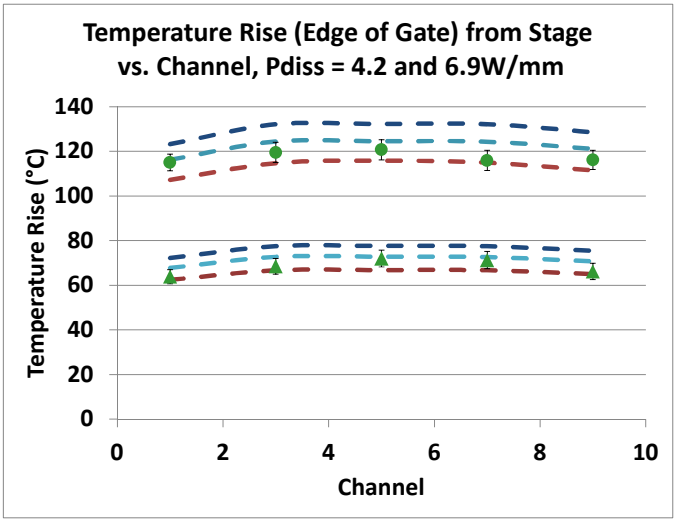

Fig.7 Measured and modeled operational temperatures for P_{diss} = 4.2 (bottom data) and 6.9W/mm (top data). The dark blue, light blue and red dashed lines represent "high", "nominal" and "low" tolerance model cases, respectively

Figure 8 shows the measured vs. modeled comparison for various channels at the center of the gate finger location. As expected, these temperatures are higher than those at the edge of the gate.

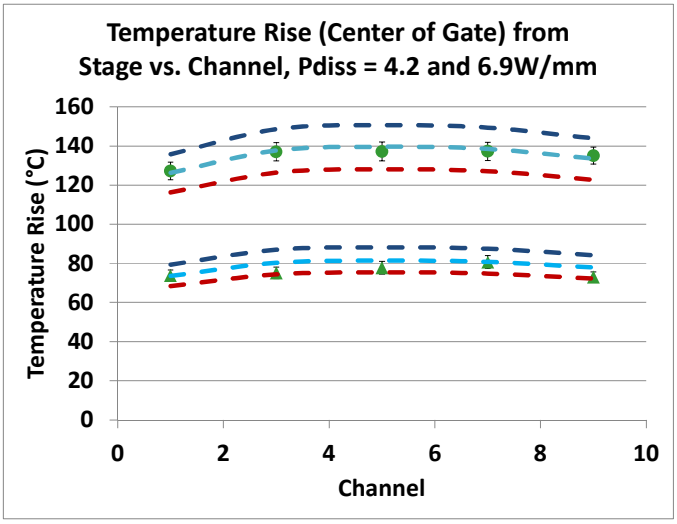

Fig.8 Measured and modeled operational temperatures for P_{diss} = 4.2(bottom) and 6.9W/mm (top). The dark blue, light blue and red dashed lines represent "high", "nominal" and "low" tolerance model cases, respectively

Figure 9 shows the modeled vs. measured comparison of thermal resistance for the center gate (Channel 5) at the edge of the gate location for varying dissipation. These results follow the expected trend of increasing thermal resistance with increasing dissipation, owing to the temperature dependent conductivity of the GaN and CVD diamond.

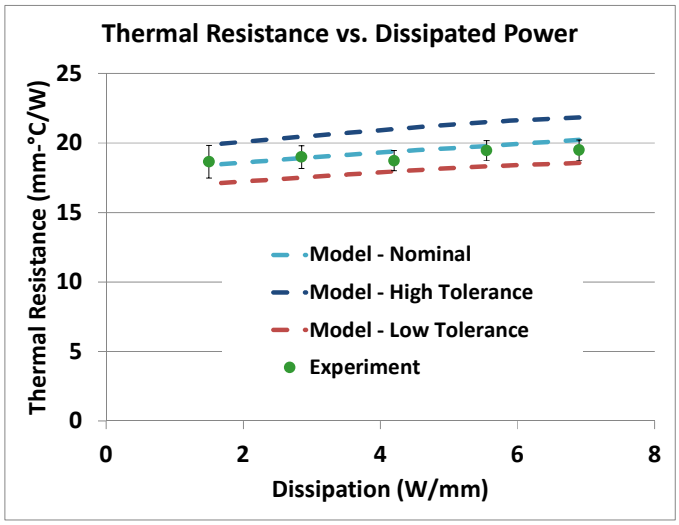

Fig.9 Measured and modeled thermal resistance, R_{th} = $(T_{measured} - T_{stage})/P_{diss}$ vs. power dissipation

Lastly, Figure 10 compares measurements and nominal modeled data for the GaN on Diamond HEMT with 10µm gate-to-gate spacing with data taken for a co-planar waveguide (CPW) GaN on SiC HEMT with a 500µm substrate and 30µm gate-to-gate spacing. It is important to note that the measurement locations for these two devices were not the same due to differences in HEMT geometry; therefore the temperatures are not directly comparable and the focus of the result is the model/experiment agreement for GaN on SiC and GaN on Diamond, which further corroborates the other Micro Raman measurements and the Gate Thermometry data.

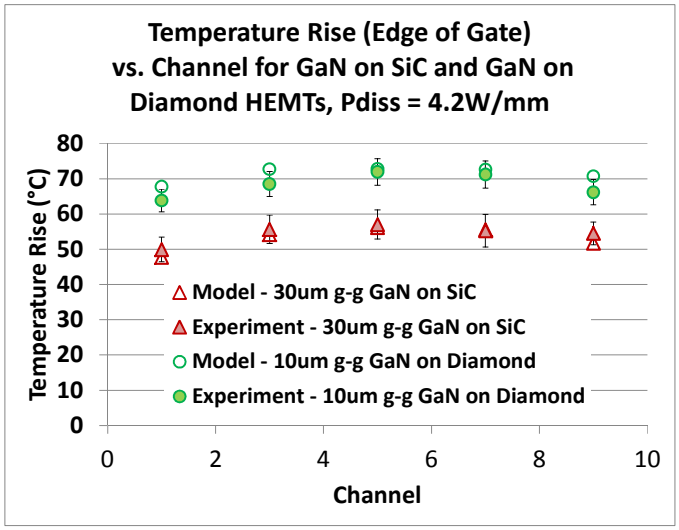

Fig.10 Measured and modeled operational temperatures of GaN on SiC and Diamond HEMTs

When viewed in their entirety, the Gate Thermometry and Micro-Raman measurements demonstrate strong agreement between modeled and measured device temperatures across multiple devices of differing type (e.g., GaN on Diamond and GaN on SiC), geometry (varying g-g spacing), device locations (edge vs. center of gate) and varying power dissipation.

Electro-thermal modeling of peak junction temperature

While both the Gate Thermometry and Micro-Raman techniques provide valuable information on device operational temperature, great care must be exercised when relating results obtained in separate measurements. This need stems from the thermal profile variations present in the near-junction region, which can vary with device type, geometry, and operating condition. Therefore, once confidence is established in the device electro-thermal model through validation, it may be most useful to compare model-predicted peak junction temperature, defined as the peak nodal temperature that occurs in the model with adequate mesh density.

As such, we employed the validated model to predict peak junction temperature and provide a comparative assessment of GaN on Diamond and GaN on SiC at a nominal dissipation of P_{diss} = 4.2W/mm (Figure 11). For 40µm gate-to-gate spacing HEMTs, the GaN on Diamond device was determined to exhibit a peak junction temperature of 90.3°C, 8.5°C (9%) lower than GaN on SiC. The GaN on Diamond HEMT device with 10µm gate-to-gate spacing was determined to exhibit a peak junction temperature of 113.8°C, 6.3°C (6%) higher than the 30µm gate-to-gate spacing GaN on SiC HEMT.

As can be seen in Figure 11, the benefit provided by GaN on Diamond stems directly from the reduced temperature drop in the device substrate, partially offset by increased temperature drop across the GaN-substrate interface (a.k.a. TIR) and packaging. The temperature drop across the packaging layers is larger in the GaN on Diamond devices due to the increased heat flux presented to the packaging. This is the result of both reduced spreading in the thinner diamond substrate and higher HEMT heat flux (for the 10µm gate-to-gate spacing device). Variations in GaN temperature drop are driven primarily by GaN thickness, with the GaN on Diamond devices featuring a ~0.4µm thinner GaN layer relative to the GaN on SiC devices.

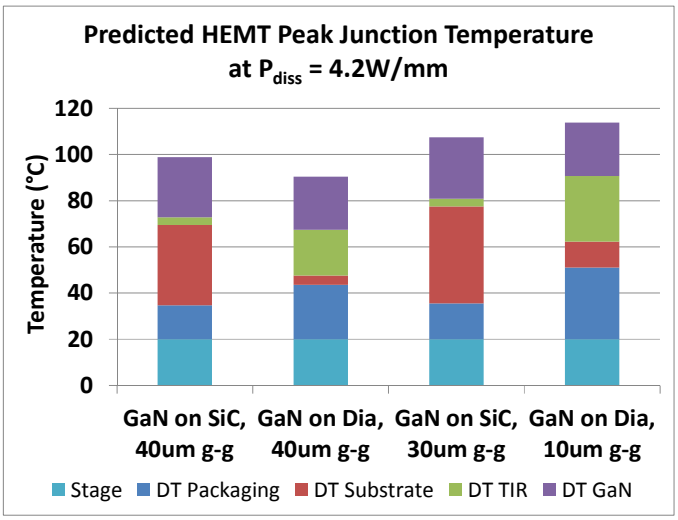

Fig.11 Model-predicted peak junction temperatures of GaN on SiC and Diamond HEMTs

Although we did not fabricate (and therefore did not measure) GaN on SiC devices with 10µm gate-to-gate spacing, follow-on simulations indicated that the peak junction temperature would increase more than 50°C relative to a 30µm gate-to-gate device. This result underscores the incremental nature of the temperature increase observed in the GaN on Diamond device for a 3X (from 140 to 420W/mm^2) increase in areal dissipation density, as well as the importance of the high conductivity diamond substrate at high HEMT areal power density.

SUMMARY & CONCLUSIONS

This study quantified and explained thermal performance benefits associated with the use of GaN on Diamond as a means to reduce operating temperature and/or increase the power density in GaN HEMTs.

A 2.7X reduction in HEMT thermal resistivity (relative to GaN on SiC) was measured using Gate Thermometry. This result was corroborated by multiple Micro-Raman measurements that profiled operational temperature in a GaN on Diamond HEMT with 3X the areal dissipation density of a baseline GaN on SiC device. Results were related by performing electro-thermal simulations featuring independently measured device and packaging characteristics.

Strong agreement was obtained between measured and modeled device temperatures across multiple device types and geometries at various locations within the HEMT and power dissipations. This strong correlation enabled use of the model to confidently predict peak junction temperature in GaN on SiC and GaN on Diamond HEMTs. These simulations revealed an incremental (6%) increase in peak junction temperature for the GaN on Diamond HEMT at 3X the areal dissipation density (420 vs. 120W/mm^2) of the baseline GaN on SiC device. Further improvement is anticipated in HEMTs fabricated on next generation GaN on Diamond substrates, which have been measured to exhibit reduced GaN-Diamond TIR (~29 vs. 47.6m^2-K/GW), such that a >3X reduction in thermal resistance is expected.

These data provide a robust demonstration of the capability of GaN on Diamond to increase HEMT power density to enable smaller, higher power density Monolithic Microwave Integrated Circuits (MMICs). Perhaps equally importantly, we have successfully related these performance advantages to underlying material characteristics, building confidence in results, and informing follow-on development and future GaN on Diamond RF device design efforts.

Acknowledgements

The authors would like to thank Dr. Avram Bar-Cohen for his leadership of the DARPA Near Junction Thermal Transport (NJTT) effort of the Thermal Management Technologies Program under which this work was performed.

This material is based upon work supported by the Defense Advanced Research Project Agency (DARPA) and US Army Contracting Command, Redstone Arsenal, AL under Contract No. W31P4Q-11-C-341.

The views expressed are those of the authors and do not reflect the official policy or position of the Department of Defense or the U.S. Government.

Distribution Statement “A” (Approved for Public Release, Distribution Unlimited) [DISTAR Case #22522]

References

[1] Y.-F. Wu, M. Moore, A. Saxler, T. Wisleder, and P. Parikh, "40-W/mm double field-plated GaN HEMTs", in IEEE 64th Device Research Conference, 2006, Conference Digest, pp. 151–152.

[2] "First GaN-on-Diamond transistor announced by Emcore, Group4 Labs, and AFRL" in Semiconductor Today, Aug 2, 2006.

[3] G.D. Via, J.G. Felbinger, J. Blevins, K. Chabak, G. Jessen, J. Gillespie, R. Fitch, A. Crespo, K. Sutherlin, B. Poling, S. Tetlak, R. Gilbert, T. Cooper, R. Baranyai, J.W. Pomeroy, M. Kuball, J.J. Maurer, and A. Bar-Cohen, "Wafer-Scale GaN HEMT Performance Enhancement by Diamond Substrate Integration" in 10th International Conference on Nitride Semiconductors, ICNS-10, August 25-30, 2013, Washington DC, USA.

[4] D.C. Dumka, T.M. Chou, J.L. Jimenez, D.M. Fanning, D. Francis, F. Faili, F. Ejeckam, M. Bernardoni, J.W. Pomeroy, and M. Kuball, "Electrical and Thermal Performance of AlGaN/GaN HEMTs on Diamond Substrate for RF Applications" in 35th IEEE Compound Semiconductor IC Symposium (CSICS) Oct 13-16 2013, Monterey, CA, Section F.4.

[5] J. Cho, Y. Li, D.H. Altman, W.E. Hoke, M. Asheghi and K.E. Goodson, "Temperature Dependent Thermal Resistances at GaN-substrate Interfaces in GaN Composite Substrates", Compound Semiconductor Integrated Circuit Symposium (CSICS) La Jolla, CA, 14-17 Oct. 2012, pp. 1-4.

[6] D. I. Babic, Q. Diduck, P. Yenigalla, A. Schreiber, D. Francis, F. Faili, F. Ejeckam, J.G. Felbinger and L.F. Eastman, "GaN-on-diamond Field-Effect Transistors: from Wafers to Amplifier Modules", MIPRO, 2010 Proceedings of the 33rd International Convention, Opatija, Croatia, 24-29 May 2010, pp. 60-66

[7] D. G. Cahill, "Analysis of heat flow in layered structures for time-domain thermoreflectance," *Rev. Sci. Instrum.*, vol. 75, no. 12, pp. 5119–5122, Nov. 2004.

[8] K.E. Goodson, "Thermal Conduction on Nonhomogeneous CVD Diamond Layers in Electronic Microstructures," ASME Journal of Heat Transfer., vol. 118, pp. 279-286, May 1996

[9] J.E. Graebner, "Measurements of Thermal Conductivity and Thermal Diffusivity of CVD Diamond," *International Journal of Thermophysics,* vol 19, No. 2, 1998, pp 511-523, 1998

[10] A. Darwish, A. Bayba and H. A. Hung, "Utilizing Diode Characteristics for GaN HEMT Channel Temperature Prediction", IEEE Trans. On Microwave Theory and Techniques, vol 56, No. 12, Dec. 2008, pp. 3188-3192

[11] T. Beechem, A. Christensen, S. Graham and D. Green, "Micro-Raman thermometry in the presence of complex stresses in GaN devices", Journal of Applied Physics, vol 103, issue 12, pp 124501-124501-1, 2008

[12] J. Pomeroy[a], M. Bernardoni[a], A. Sarua[a], A. Manoi[a], D.C. Dumka[b], D.M. Fanning[b], M. Kuball, "Achieving the Best Thermal Performance for GaN-on-Diamond," in 35th IEEE Compound Semiconductor IC Symposium (CSICS) Oct 13-16 2013, Monterey, CA, Section H.4.

[13] Y. S. Touloukian and E. H. Buyco, "Thermophysical Properties of Matter: Specific Heat: Metallic Elements and Alloys," John Wiley & Sons Ltd, 1970.

[14] Y. S. Touloukian and E. H. Buyco, "Thermophysical Properties of Matter: Specific Heat: Metallic Elements and Alloys," John Wiley & Sons Ltd, 1970.

[15] J. E. Graebner, "Measurements of specific heat and mass density in CVD diamond," Diam. Rel. Mater., vol. 5, no. 11, pp. 1366–1370, Nov. 1996.

[16] D. G. Cahill et al., "Nanoscale thermal transport. II. 2003–2012," Applied Physics Reviews, vol. 1, no. 1, pp. 011305, 2014.

[17] J. Cho, Y. Li, W. E. Hoke, D. H. Altman, M. Asheghi, and K. E. Goodson, "Phonon scattering in strained transition layers for GaN heteroepitaxy," Phys. Rev. B, Condens. Matter, vol. 89, no. 11, pp. 115301-1-115301-11, Mar. 2014.

[18] J. Cho, E. Borzorg-Grayeli, D. Altman, M. Asheghi and K. Goodson, " Low Thermal Resistances at GaN-SiC Interfaces for HEMT Technology," *IEEE Electron Device Letters*, Vol. 33, No. 3, pp 378-380, March 2012.

[19] A. Manoi, J. Pomeroy, N. Killat and M. Kuball, "Benchmarking of Thermal Boundry Resistance in AlGaN/GaN HEMTs on SiC Substrates: Implications of the Nucleation Layer Microstructure," *IEEE Electron Device Letters*, Vol. 31, No. 12, pp 1395-1397, December 2010.

[20] A.Sukhadolau, E. Ivakin, V. Ralchenko, A. Kohomich, A. Vlasov and A. Popovich, " Thermal conductivity of CVD diamond at elevated temperatures," *Diamond and Related Materials*, Vol. 14, pp. 589-593, 2000

[21] S. Coe and R. Sussman, "Optical, thermal and mechanical properties of CVD diamond," *Diamond and Related Materials*, Vol 9, pp. 1726-1729, 2000

[22] D. Altman, M. Tyhach, J. McClymonds, S. Kim, S. Graham, J. Cho, K. Goodson, D. Francis, F. Faili, F. Ejeckam, and S. Bernstein, "Analysis and Characterization of Thermal Transport in GaN GEMTs on SiC and Diamond Substrates," GOMACTech 2014, Charleston SC, April 2014, in press